ACS APPLIED MATERIALS & INTERFACES

Research Article

www.acsami.org

Monitoring of the Enzymatic Degradation of Protein Corona and Evaluating the Accompanying Cytotoxicity of Nanoparticles

Zhifang Ma,[†,‡] Jing Bai,[†] and Xiue Jiang*[,†]

[†]State Key Laboratory of Electroanalytical Chemistry, Changchun Institute of Applied Chemistry, Chinese Academy of Science, Changchun, Jilin 130022, P. R. China

[‡]University of Chinese Academy of Sciences, Beijing 100049, P. R. China

Supporting Information

ABSTRACT: Established nanobio interactions face the challenge that the formation of nanoparticle−protein corona complexes shields the inherent properties of the nanoparticles and alters the manner of the interactions between nanoparticles and biological systems. Therefore, many studies have focused on protein corona-mediated nanoparticle binding, internalization, and intracellular transportation. However, there are a few studies to pay attention to if the corona encounters degradation after internalization and how the degradation of the protein corona affects cytotoxicity. To fill this gap, we prepared three types of off/on complexes based on gold nanoparticles (Au NPs) and dye-labeled serum proteins and studied the extracellular and intracellular proteolytic processes of protein coronas as well as their accompanying effects on cytotoxicity through multiple evaluation mechanisms, including cell viability, adenosine triphosphate (ATP) content, mitochondrial membrane potential (MMP), and reactive oxygen species (ROS). The proteolytic process was confirmed by recovery of the fluorescence of the dye-labeled protein molecules that was initially quenched by Au NPs. Our results indicate that the degradation rate of protein corona is dependent on the type of the protein based on systematical evaluation of the extracellular and intracellular degradation processes of the protein coronas formed by human serum albumin (HSA), γ-globulin (HGG), and serum fibrinogen (HSF). Degradation is the fastest for HSA corona and the slowest for HSF corona. Notably, we also find that the Au NP-HSA corona complex induces lower cell viability, slower ATP production, lower MMP, and higher ROS levels. The cytotoxicity of the nanoparticle-protein corona complex may be associated with the protein corona degradation process. All of these results will enrich the database of cytotoxicity induced by nanomaterial-protein corona complexes.

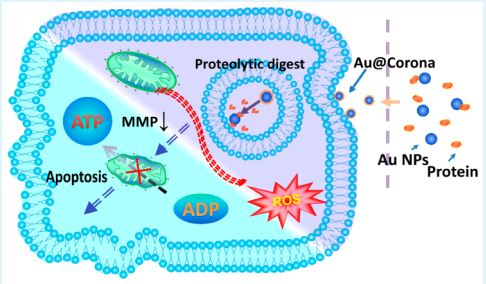

KEYWORDS: *Au nanoparticles, protein corona, ATP, mitochondrial membrane potential, reactive oxygen species*

1. INTRODUCTION

Advances in nanotechnology have accelerated the translation of nanomaterials into the field of biomedicine.[1] To address their efficacy and safety issues, the interactions between engineered nanoparticles and biological systems have been extensively investigated. It is generally accepted that the variations in physicochemical characteristics, such as compositions, size, shape, surface chemistry, and aggregation play a crucial role in determining their interactions with biomolecules, cells, and tissues.[2−5] However, the established nanobio interactions face a tremendous challenge because of the complexity of biological systems. For instance, nanomaterials injected into the bloodstream will come into contact with a mixture of diverse cells and extracellular proteins and subsequently form nanoparticle−protein corona complexes, which will critically impact the biological identities of nanoparticles and change the biological responses to nanoparticles.[6−12]

A protein corona can be formed on the surface of metal and oxide nanoparticles,[13−15] silica nanoparticles,[16,17] polymeric nanoparticles,[8,18] quantum dots,[19−21] and so forth. The formation of the corona is a dynamic and competitive process that is determined by the affinity of the protein for the surface.[6,22,23] The weakly bound, low-affinity proteins will form the "soft corona", and the tightly bound, high-affinity proteins will form the "hard corona".[6,24] Over 70 serum proteins have been identified in a protein corona around the surface of gold nanoparticles.[25] The compositions of the protein corona can evolve with the microenvironment.[26,27] The cellular responses to the nanoparticles, such as the cellular targeting and uptake, will be dramatically changed by the protein corona, which also changes the biological fate of the same particles, such as subcellular localization and retention time.[7,14,25,28−32] Bovine serum albumin (BSA) corona will enhance the cellular binding of cationic nanoparticles while inhibiting the cellular binding of anionic nanoparticles.[6] Most importantly, the protein corona also plays a protective role with respect to the toxic effects of nanomaterials. For instance, the adsorbed proteins largely reduce the effect of graphene oxide nanosheets[30] and carbon

Received: January 6, 2015
Accepted: July 22, 2015
Published: July 22, 2015

DOI: 10.1021/acsami.5b05744
ACS Appl. Mater. Interfaces 2015, 7, 17614−17622

nanotubes[31] on cell viability, and silica nanoparticle-protein corona complexes have less effect on cellular adhesion compared to that of uncoated nanoparticles.[24] A protein corona also reduces reactive oxygen species.[13] Nevertheless, there is still a gap between protein corona-mediated nanoparticle binding, internalization, intracellular transportation, and cytotoxicity.

It is well-known that many kinds of proteinases distributed in the cytoplasm and organelles can efficiently degrade protein molecules. These proteolytic enzymes might degrade protein coronas when the nanoparticle−protein corona complexes are internalized by the cells, which might motivate or change some related metabolism processes and result in cytotoxicity. However, very limited attention has been paid to the effect of enzymatic degradation of the protein corona on the cytotoxicity of the nanoparticle-corona complex.[33] A delayed toxicity has been observed for the protein corona-protected cationic nanoparticles, corresponding to the degradation of the corona inside the lysosomes and the re-exposition of the toxic surface.[34] To fill the gap in tracing the effects of the protein corona on the cytotoxicity of nanoparticles, we prepared the Au NP-protein corona complexes by selecting three major serum proteins, HSA, HGG, and HSF, as the model proteins. The corona protein was labeled by fluorescence dye. In the Au NP-protein corona complexes, the emission of the dye can be quenched by Au NPs because the emission of the dye overlaps with the localized surface plasmon resonance (LSPR) band of Au NPs. However, it can be recovered after detaching from the surface of Au NPs due to enzymatic degradation. Such an off/on property enables us to monitor in situ the extracellular and intercellular enzymatic degradation process. The accompanying cytotoxicity consequence related to this process has been evaluated by multiple assays, including cell viability, LDH leakage, ATP content, MMP, and ROS. Our data highlight the importance of using multiple assays to evaluate the cytotoxicity of the nanoparticle-protein corona complex.

2. EXPERIMENTAL SECTION

Chemicals. Sodium citrate was obtained from Beijing Chemical Reagents Company (China). Proteinase K was purchased from Aladdin Reagents Company (China). Dulbecco's modified Eagle's medium (DMEM) was purchased Thermo Scientific (Beijing, China). Calcium- and magnesium-free Dulbecco's phosphate-buffered saline (PBS) was obtained from Invitrogen. Sodium gold chloride ($NaAuCl_4$), HSA (A1653), HGG (G5385), HSF (F-4883), and fluorescein isothiocyanate (FITC, F4274) were purchased from Sigma Chemical Company. Deionized (D.I.) water was generated using a Millipore Milli-Q system (Billerica, MA). All chemicals were used without additional purification.

Preparation of Citrate-Stabilized Au Nanoparticles. Au NPs were prepared according to the Frens' method.[34] Typically, aqueous $NaAuCl_4$ solution (100 mL, 5×10^{-4} M) was heated to boiling, and then aqueous sodium citrate solution (1% w/w, 5 mL) was added as quickly as possible to this solution under vigorous stirring. The mixed solution was continually heated for 15 min under stirring until the color of the solution turned ruby red. The synthesized nanoparticle solution was cooled to room temperature and then stored at 4 °C for further use. The as-prepared Au NPs were characterized with transmission electron microscopy (TEM) on an H-600 electron microscope (Hitachi, Japan), UV−vis spectrometer LAMBDA 25 (PerkinElmer, Germany), and dynamic light scattering using a Zetasizer (ZEN3600, Malvern Co., UK).

Preparation of FITC-Labeled Serum Protein. The free ε-lysine residue of the protein molecule can connect with FITC through a covalent reaction. Typically, HSA, HGG, and HSF were separately dissolved in sodium bicarbonate buffer (25 mM, pH 9.8) at a concentration of 1.33 mg/mL. The protein solution (15 mL) was then enclosed in a cellulose ester dialysis membrane bag (Pierce, MWCO 3500), and the bag was suspended in 800 mL of sodium bicarbonate buffer solution (25 mM, pH 9.8). After that, FITC (2 mg) was added to the dialysis buffer solution, and the solution was stirred for 24 h in the dark. The reaction was terminated by dialysis against PBS (pH 7.4). To remove the unreacted FITC completely, we replaced the PBS every 12 h over the course of 72 h. Finally, the obtained FITC-labeled protein solution was diluted to 20 mL (1 mg/mL) with PBS (pH 7.4) and stored at 4 °C for further use.

Synthesis of Protein-Coated Au NPs. The pH of the Au NP solution was adjusted to 7−8 with NaOH, and then, the labeled-protein solution (1 mL) was added dropwise to 20 mL of the gold nanoparticle solution ($[Au^0]$ = 500 μM) under vigorous stirring. The reaction mixture was stirred for 24 h in the dark to form gold nanoparticle-protein corona complexes (Au@Protein-FITC NPs). After that, the complexes were purified via centrifugation (10000*g*, 30 min), and the centrifugation steps were repeated until no fluorescence was measured in the discarded supernatants. The obtained Au@Protein-FITC NPs were resuspended into 20 mL of PBS and stored at 4 °C for further use. Au@Protein NPs were prepared using the same strategy and characterized with TEM, UV−vis spectrometry, and dynamic light scattering.

Enzymatic Degradation of the Protein Corona in Buffer. The extracellular degradation of the protein corona was carried out by coincubation of proteinase K with the Au@Protein-FITC NP solution in PBS (pH 7.4) at 37 °C. The fluorescence of FITC-labeled protein corona was initially quenched by Au NPs. After coincubating with proteinase K, the corona was gradually degraded into fragments and released into the solution with incubation time, resulting in the recovery of the fluorescence of the quenched FITC molecules. The fluorescence of the FITC molecule in the supernatant could be detected by a fluorescence spectrometer. Typically, proteinase K dissolved in PBS (200 μL, 5 mg/mL) was added to 5 mL of the Au@Protein-FITC NP solution, and the mixture was kept at 37 °C and pH 7.4 for 24 h under stirring. At selected time intervals (0, 1, 2, 3, 4, 8, 16, and 24 h), aliquots were removed and centrifuged, and the fluorescence intensity of the supernatant was measured with a fluorescence spectrometer (LS-55, PerkinElmer, Germany) to evaluate the degradation process. At 24 h, the aliquots were also removed for UV−vis spectroscopy measurements.

Confocal Microscopy Measurements. HeLa cells (human cervical cancer cell line) were maintained in DMEM medium supplemented with 10% fetal bovine serum and 1% penicillin and streptomycin. The culture flask was incubated in a humidified incubator with 5% CO_2 at 37 °C. Prior to measurements, HeLa cells were seeded in cell culture dishes (Ø 20 mm, NEST Biotech Co., Ltd., China) and cultured in 5% CO_2 at 37 °C for 24 h at a density of 1×10^6 cells. Then, the cells were washed with PBS solution three times. Afterwards, Au@HSA-FITC, Au@HGG-FITC, and Au@HSF-FITC NPs (1 mL, 625 nM) were added to the culture dishes immediately after being suspended in culture medium, and the cells were imaged using a confocal laser scanning fluorescence microscope (CLSM, Leica TCS SP2, Leica Microsystems, Mannheim, Germany) with a 100× objective at different time points (0, 30, 120, 240, 360, 480 min). After a 1 h incubation, the cells were rinsed with PBS solution to sufficiently remove the extracellular nanoparticles and incubated with fresh medium. The culture dish was fixed at the same position to ensure that the same cells were imaged throughout the process. The cells cultured in medium without particles throughout were used as the control. FITC was excited at 488 nm and observed through a 500−550 nm emission band-pass filter. The mean fluorescence intensity at each time point was calculated using ImageJ software from 20 cells in three separate experiments.

Inductively Coupled Plasma Mass Spectrometry (ICP−MS) Measurement. HeLa cells were seeded in cell culture dishes (Ø 20 mm, NEST Biotech Co. ltd, China) and cultured in 5% CO_2 at 37 °C for 24 h at a density of 1×10^6 cells. Subsequently, the cells were washed with PBS solution three times, and then, Au, Au@HSA-FITC,

DOI: 10.1021/acsami.5b05744
ACS Appl. Mater. Interfaces 2015, 7, 17614−17622

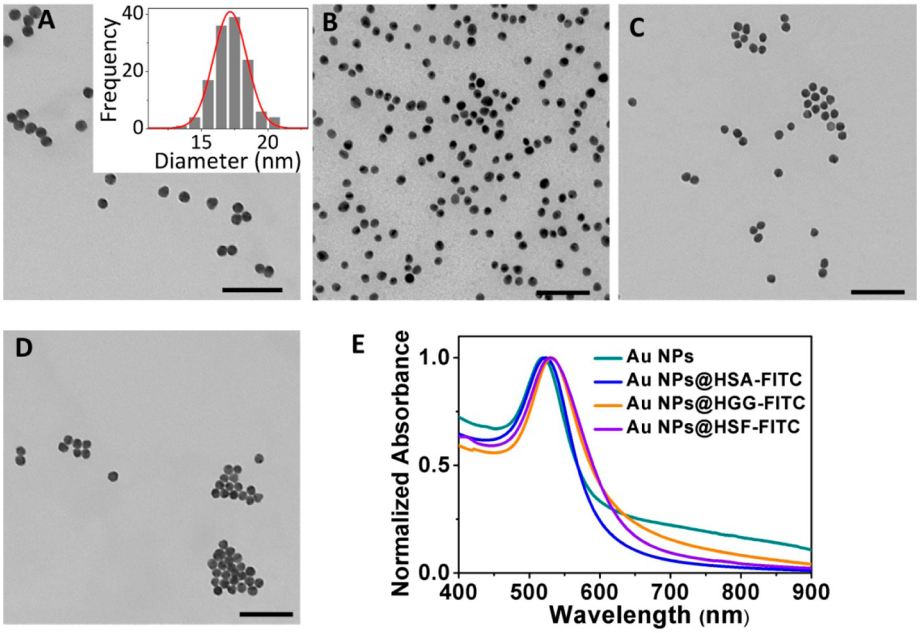

Figure 1. TEM images of (A) citrate-stabilized Au NPs, (B) Au@HSA-FITC NPs, (C) Au@HGG-FITC NPs, and (D) Au@HSF-FITC NPs (Inset: histogram of the size distribution of the Au NPs). (E) UV−vis spectra of aqueous Au NPs (cyan), Au@HSA-FITC NPs (blue), Au@HGG-FITC NPs (orange), and Au@HSF-FITC NPs (purple) solutions. The scale bar in A−D corresponds to 200 nm.

Au@HGG-FITC, and Au@HSF-FITC NPs (1 mL, 625 nM) were added to the culture dishes immediately after being suspended in culture medium. The cells were incubated for 1 h at 37 °C with 5% CO_2. After being thoroughly rinsed with PBS solution to remove free nanoparticles in the medium, the cells in each dish were trypsinized and collected into a polypropylene centrifuge tube. The content of Au was measured with ICP-MS (DIONEX ICS-1000, USA).

Cell Viability Assay. The viability of cells after treatment with Au NPs or Au@Protein NPs was evaluated by a methylthiazoleterazolium (MTT) assay. In brief, HeLa cells were seeded in a 96-well microliter plate at a density of 1×10^4 cells per well and allowed to attach for 24 h at 37 °C in 5% CO_2. At ∼80% confluency, the cells were washed three times with PBS and subsequently incubated with Au NPs and Au@Protein NPs at different concentrations (0, 32, 64, 125, 250, and 500 μM) in the cell medium for 24 h at 37 °C in 5% CO_2. A control experiment was similarly performed in the absence of nanoparticles. Afterwards, the cells were washed by PBS three times, and MTT dissolved in the cell medium (100 μL, 0.5 mg/mL) was added to each well. After incubation for 4 h at 37 °C in 5% CO_2, the medium was then replaced with 100 μL of dimethyl sulfoxide (DMSO). Then, the 96-well culture plate was shaken several times to thoroughly dissolve the formazan in DMSO. The absorbance at 570 nm was measured with a Synergy HT Multimode Microplate Reader (Bio-Tek Instruments, Inc., Winooski, VT, USA). The percentage of cell viability was calculated according to $A_{570}/A_{570(control)} \times 100\%$.

Detection of ATP, MMP, and ROS. HeLa cells were plated in a 6-well microliter plate at a density of 1×10^6 cells per well and allowed to attach for 24 h at 37 °C in 5% CO_2. At ∼80% confluency, the cells were exposed to either Au and Au@Protein NPs dispersed in the fresh culture medium at the concentration of 500 μM or exposed to fresh culture medium as a control for 3 h at 37 °C in 5% CO_2. Afterwards, the cells were washed with PBS and used for ATP, MMP, and ROS measurements with ATP, MMP, and ROS assay kits (Beyotime Biotechnology).

For ATP detection, lysis buffer (400 μL) was added to each well to lyse the cells. The lysed cells were collected into a polypropylene centrifuge tube and centrifuged at 10000*g* for 5 min, and the supernatant was collected for the following measurements. ATP test solution (100 μL) was added to each well of a 96-well microliter plate and kept for 5 min to deplete the ATP of the background. Then, the lysed cell supernatant (100 μL) was added to the test solution in each well, mixing well through rapid pipetting. The luminescence intensity was determined by a Multimode Microplate Reader (Bio-Tek Instruments, Inc., Winooski, VT, USA), and the results were expressed as a percentage of the control.

For detection of MMP, JC-1 staining solution (1 mL) was added to each well, and the cells were incubated at 37 °C in 5% CO_2 for 30 min. After being washed with PBS three times, cells in each well were trypsinized and resuspended with 400 μL of JC-1 buffer. The cell suspension was added to a 96-well microliter plate, and the fluorescence emission of the cell suspension was measured on a Multimode Microplate Reader (Bio-Tek Instruments, Inc., Winooski, VT, USA) at 530 nm (JC-1 monomer) and 590 nm (JC-1 aggregate). The relative value of I_{590}/I_{530} was used to evaluate the MMP, and the results were expressed as a percentage of the control.

For ROS detection, 2′,7′-dichlorofluorescein diacetate (DCFH-DA) solution (1 mL, 10 μM) was added to each culture well, and the cells were incubated at 37 °C in 5% CO_2 for 20 min. Cells in each well were washed with PBS three times to remove free DCFH-DA. Then, the cells in each well were trypsinized and resuspended with 500 μL of culture medium without serum. The cell suspension was added to a 96-well microliter plate. The fluorescence intensity at 525 nm was determined by a Multimode Microplate Reader (Bio-Tek Instruments, Inc., Winooski, VT, USA), and the results were expressed as a percentage of the control.

3. RESULTS AND DISCUSSION

Fabrication and Characterization of Au@Protein-FITC NPs. Au NPs stabilized by citrate sodium were synthesized according to the Frens method. As shown in Figure 1A, the as-prepared NPs are monodispersed with an average diameter of 16.9 nm (inset) determined from TEM. The Au@Protein-FITC NPs were synthesized by adding the labeled protein solution to citrate-stabilized Au NPs ($[Au^0]$ = 500 μM) under vigorous stirring to coat Au NPs with preformed FITC-labeled HSA, HGG, and HSF. The FITC was covalently bonded to the protein through a nucleophilic reaction. As shown in Figure 1B−D, the Au NPs coated by HSA (Au@HSA-FITC NPs) still maintain good dispersibility, whereas coating with HGG (Au@HGG-FITC NPs) or HSF (Au@HSF-FITC NPs) seemingly

DOI: 10.1021/acsami.5b05744
ACS Appl. Mater. Interfaces 2015, 7, 17614−17622

induces slight aggregation of the Au NPs. To exactly demonstrate the characteristics of the nanoparticles in solution, we measured their zeta potentials and dynamic light scattering (DLS) diameters (Figure S1). The mean zeta potentials of Au NPs is changed from −53 mV to approximately −30 mV after coating serum proteins, and the DLS diameters are 21 ± 1, 35 ± 1, 37 ± 2, and 39 ± 1 nm for Au NPs, Au@HSA-FITC NPs, Au@HGG-FITC NPs, and Au@HSF-FITC NPs (Figure S1B–E). These results reveal the good dispersibility of Au@Protein-FITC NPs in solution. The Au@Protein-FITC NPs were further characterized by UV–vis spectroscopy. As shown in Figure 1E, the as-prepared Au NPs show the LSPR peak at 519 nm, whereas coating with HSA, HGG, and HSF results in a slight shift of the LSPR peak to 522, 531, and 529 nm, suggesting the formation of the protein corona.

Extracellular Degradation of the Protein Corona. The Au@Protein corona complex might be degraded by proteolytic enzymes distributed in organelles after their internalization by cells. Here, we simulated the degradation of the protein corona around the Au NPs by coincubation of the Au@Protein-FITC NPs with 200 μg mL^{-1} of proteinase K in PBS at 37 °C and pH 7.4 for 24 h under stirring, and characterized the dispersions with UV–vis spectroscopy (Figure 2A). Compared with the

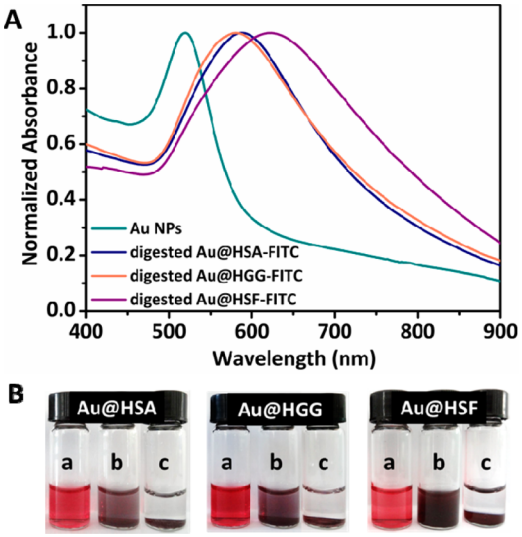

Figure 2. (A) UV–vis spectra of Au NPs after the protein corona was digested by proteinase K (200 μg mL^{-1}) in PBS (pH 7.4) at 37 °C: Au NPs (cyan), Au@HSA-FITC NPs (blue), Au@HGG-FITC NPs (orange), and Au@HSF-FITC NPs (purple). (B) Photographs of aqueous Au@Protein solutions (a) before beingdigested, (b) after being digested for 24 h under stirring, and (c) after standing for 12 h after having been digested for 24 h under stirring.

spectrum of aqueous Au NPs solution (cyan), the LSPR bands of the digested Au@HSA-FITC NPs (blue), Au@HGG-FITC NPs (orange), and Au@HSF-FITC NPs (purple) dispersions broaden and red-shift to 581, 588, and 623 nm. Correspondingly, the color of the aqueous Au@Protein NP solution is changed from ruby red (Figure 2B, a) to red-brown (Figure 2B, b). After stopping stirring for 12 h, all nanoparticles precipitate to the bottom of the vial (Figure 2B, c), indicating significant aggregation. These results indicate that the degradation of the protein corona will decrease the stability of the nanoparticles and lead to aggregation due to disturbance of the protective layer.

Furthermore, we characterized the degradation process by fluorescence spectroscopy. For the Au NPs@protein corona complex, the emission of the FITC can be completely quenched by Au NPs (Figure 3A) because the maximal

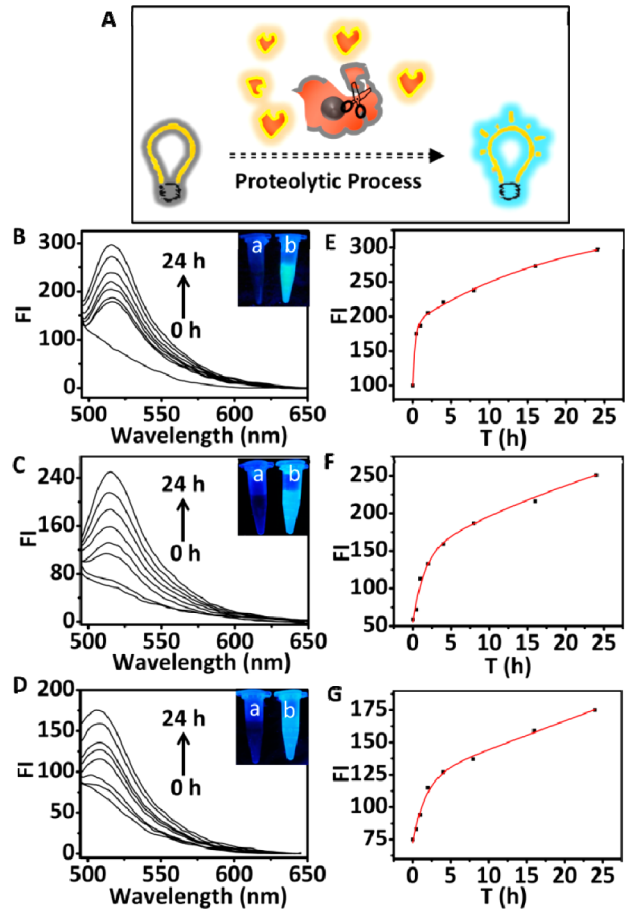

Figure 3. (A) Scheme of the fluorescence off/on for the Au@Protein-FITC NPs. Time-dependent fluorescence spectra of the released FITC upon enzymatic digestion of the protein corona for (B) Au@HSA-FITC NPs, (C) Au@HGG-FITC NPs, and (D) Au@HSF-FITC NPs. The peak fluorescence intensity of FITC after being detached from the surface of (E) Au@HSA-FITC NPs, (F) Au@HGG-FITC NPs, and (G) Au@HSF-FITC NPs plotted as a function of time and the corresponding curve fitting (red). Inset: photographs of the complexes (a) before and (b) after the proteolytic process under illumination with UV light.

emission of the FITC (λ_{max} (emission) = 520 nm) overlaps with the LSPR band of Au NPs (Figure 1E). Co-incubation of the Au NPs@protein corona complex with proteinase K results in the recovery of the fluorescence emission of the FITC (Figure 3A) due to the release of FITC from the surface of Au nanoparticles upon degradation of the protein corona. Such off/on property enables us to monitor in situ the enzymatic degradation process both extracellularly and intracellularly. The Au@Protein-FITC NPs were incubated with proteinase K in PBS at 37 °C and pH 7.4, and the fluorescence emission of the supernatant of the mixture at different times (0, 1, 2, 3, 4, 8, 16, and 24 h) was recorded (Figure 3B–D). The emission peaks gradually appear and increase in their intensities with elapsed time, suggesting the release of FITC from the surface of the Au nanoparticles due to degradation of the protein corona. The corresponding emission intensity plotted as a function of

DOI: 10.1021/acsami.5b05744
ACS Appl. Mater. Interfaces 2015, 7, 17614–17622

incubation time was shown in Figure 3E−G. The data can be fitted well with the double exponential expression[35] with residual square correlation coefficient (R^2) > 0.99.

$$F = A_1\exp(-t/k_1) + A_2\exp(-t/k_2) + F_0 \quad (1)$$

where the parameters of F and F_0 represent the fluorescence intensity at time t and the maximum fluorescence intensity when the corona is completely degraded, respectively. F_0 is proportional to the adsorption amount of protein onto Au NPs and labeled amount of FITC to the different proteins. On the basis of F_0, the value of the half-life, $t_{1/2}$, a time required for degrading half of the corona, can be read from the fitted line. As shown in Table 1, $t_{1/2}$ is 4.4, 20.5, and 73.4 h for Au@HSA-FITC NPs, Au@HGG-FITC NPs, and Au@HSF-FITC NPs, indicating a progressive decrease in their degradation rate. The maximum fluorescence intensities F_0 are 342.9, 418.7, and 431.7 for the HSA, HGG, and HSF corona.

Table 1. Degradation Kinetics Parameters of the Proteolytic Process in PBS (pH 7.4) at 37 °C

protein	F_0	$t_{1/2}$ (h)
HSA	342.9	4.4
HGG	418.7	20.5
HSF	431.7	73.4

In complex biological systems, adsorption competition by other protein and sulfhydryl compounds may also result in fluorescence recovery of the labeled protein corona.[36,37] To evaluate it, we used DMEM supplemented with serum alone and DMEM supplemented with serum and glutathione as model biological systems. Competitive adsorption was studied by incubating Au@Protein-FITC NPs with these two mediums and measuring the fluorescence of the supernatant at different time points (Figure S2). The fluorescence intensity only increases within 0.5 h for both cases. Continual incubation does not induce any increase in the fluorescence intensity of the supernatant for all Au@Protein-FITC NPs even after 24 h, which indicates that competitive adsorption does indeed happen but only partially recovers the quenched fluorescence rapidly.

The enzymatic degradation processes of the Au@Protein-FITC NPs in the DMEM supplemented by 10% fetal bovine serum and glutathione were further investigated by coincubation of the Au@Protein-FITC NPs with medium in the presence of proteinase K (Figure S3A−C). The fluorescence intensity is continually increased during the experimental period even after 0.5 h, indicating that the enzymatic degradation mainly contributes to the recovery of the quenched fluorescence even in the presence of competitive adsorption in a complex system. The maximum fluorescence intensities F_0 (Table S1) for Au@HSA-FITC NPs, Au@HGG-FITC NPs, and Au@HSF-FITC NPs obtained by fitting the fluorescence intensities after 0.5 h (Figure S3D−F) with eq 1 are very close to those when Au@Protein-FITC NPs are enzymatic degraded in PBS. Their degradation rate also shows the same tendency as that in PBS, although the values of $t_{1/2}$ for Au@HSA-FITC NPs, Au@HGG-FITC NPs, and Au@HSF-FITC NPs are several times longer (Table S1) due possibly to the adsorption competition results in areas where the enzyme has less access to the corona.

Intracellular Degradation of the Protein Corona. The recovery of the fluorescence emission due to the release of FITC from the surface of the plasmonic Au NPs was also observed in living HeLa cells. The cells were incubated with 625 nM of Au@HSA-FITC, Au@HGG-FITC, and Au@HSF-FITC NPs and imaged at 0, 30, 120, 240, 360, 480 min, using CLSM (Figure 4). For the cells incubated with Au@HSA-FITC and Au@HGG-FITC NPs, the bright spots could be observed at 30 min. To remove the extracellular nanoparticles, we sufficiently rinsed the cells with PBS solution after 1 h incubation and reincubated the cells with fresh medium. For the Au@HSA-FITC and Au@HGG-FITC NPs-treated cells, the cellular fluorescence gradually increased over time, although the intensity is different. However, for the Au@HSF-FITC NPs-treated cells, the cellular fluorescence was observed only after 240 min. The recovery of the FITC fluorescence in the living HeLa cells meant that all three types of the protein

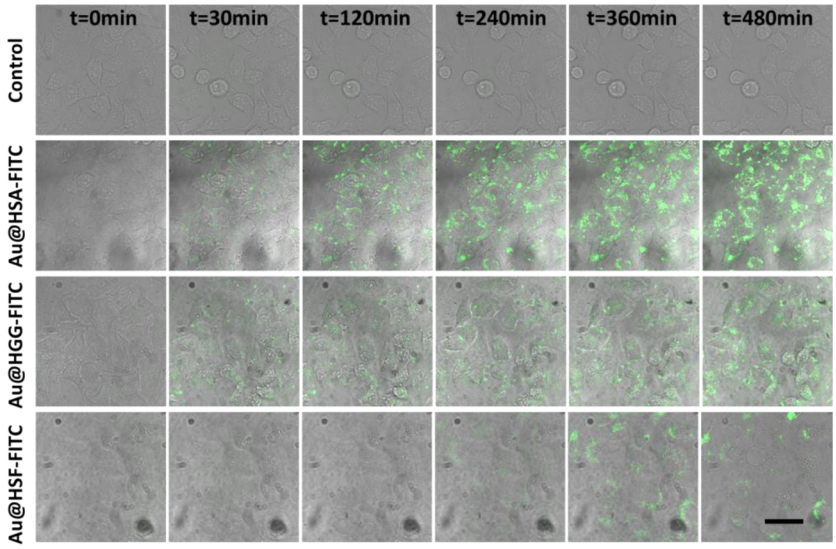

Figure 4. Time-dependent confocal fluorescence and bright-field (overlay) images of HeLa cells after being treated with PBS as control, 625 nM Au@HSA-FITC NPs, Au@HGG-FITC NPs, and Au@HSF-FITC NPs in PBS at 37 °C. All the NPs were washed away at 1 h, and the cells were incubated with fresh medium. Scale bars: 20 μm.

DOI: 10.1021/acsami.5b05744
ACS Appl. Mater. Interfaces 2015, 7, 17614−17622

coronas were biologically degradable upon enzymatic digestion. However, the difference in the fluorescence intensity and the time point that brightness patterns appeared in the cells could result from differences in the uptake amounts of different NPs, the amount of absorbed FITC, and/or the intracellular degradation kinetics. To identify the origin of the difference, we quantified the uptake amounts of Au, Au@HSA, Au@HGG, and Au@HSF NPs by HeLa cells by measuring the Au content with ICP−MS (Figure 5A). The amounts of the Au@HSA, Au@HGG, and Au@HSF NPs internalized by HeLa cells are much less than that of the internalized Au NPs, but there are no significant differences amongst one another. Therefore, it is reasonable to consider that the recovery of fluorescence in the cells is largely determined by the detachment rate of the adsorbed FITC from the surface of the Au NPs. Figure 5B shows the mean fluorescence intensity (MFI) of each cell image as a function of the incubation time. Because the labeled amount of FITC on each protein molecule will affect the fluorescence intensity, the MFI was subsequently normalized by the values of F_0 in Table 1 to eliminate the effect of the adsorption amount of FITC on the MFI (Figure 5C). After normalization, the increase of MFI for the cells treated with Au@HSA-FITC is obviously faster than those of the cells treated with the other two particles, indicating that the proteolytic process of the HSA corona has been performed on a larger scale than the other two protein coronas in living cells within the observed time scale.

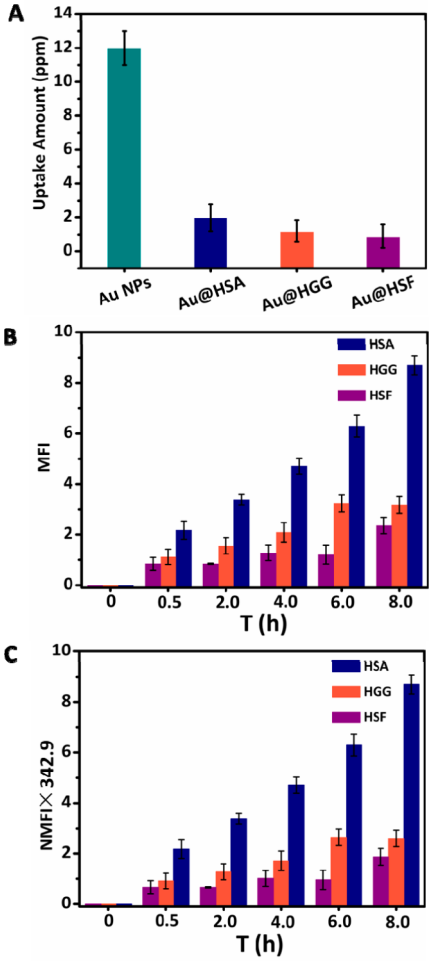

Figure 5. (A) Uptake amount of Au NPs and Au@protein coronas as determined from the measured Au content with ICP-MS. (B) The mean fluorescence intensity of cells treated with Au@HSA, Au@HGG, and Au@HSF NPs analyzed from 20 cells in three separate experiments using ImageJ software. (C) The mean fluorescence intensity of cells normalized with the maximum fluorescence intensity F_0 obtained from curve fitting of Figure 3. Error bars indicate standard deviations from the mean.

Evaluation of the Cytotoxicity of Gold Nanoparticles-Protein Corona. To evaluate the effects of the Au NPs-protein corona on the cytotoxicity, we first determined the viability of the HeLa cells after exposure to Au, Au@HSA, Au@HGG, and Au@HSF NPs at a concentration range of 32−500 μM for 24 h by MTT assay (Figure 6A). There is no acute effect on the cell viability when the concentration of the exposed Au NPs is <250 μM because more than 90% of the cells are viable. However, when the incubation concentration of the Au NPs was increased to 500 μM, the cell viability is significantly decreased to 80%, indicating a dose-dependent cytotoxicity. After the particles were coated with protein, only the viability of the cells treated with Au@HGG and Au@HSF NPs has an obvious increase in comparison with that of the cells treated with uncoated Au NPs ($P < 0.05$), whereas the Au@HSA NPs have nearly the same effect on the cell viability as that of the uncoated Au NPs. At the studied concentration range, the HSF corona has an obvious role in improving the biocompatibility of the Au NPs compared with that of HSA corona. The results match the trend of the degradation rate of protein corona extracellularly and intracellularly, suggesting a possible relationship between the cell viability and the corona proteolytic process. Protein corona with a slower degradation rate may have an obvious protection against the effect of the nanomaterials on cell viability.

Because the assessment of cell viability with an MTT assay is based on the evaluation of the ability of viable cells to reduce MTT into formazan by mitochondrial succinate dehydrogenase, and thus, its results cannot fully reflect the cell growth state, it is far from being enough to evaluate cytotoxicity induced by NPs.[38,39] To obtain a fuller understanding on the effect of protein corona on cytotoxicity, we further performed experiments related to other important events for assessment of cytotoxicity, including LDH leakage, producion of ATP (Figure 6B), loss of MMP (Figure 6C), and production of ROS (Figure 6D).

The LDH leakage assay is often used to evaluate the integrity of a cell membrane based on the measurement of lactate dehydrogenase activity in the extracellular medium.[40] In comparison with cells treated with 0.25% Triton-X-100 (positive control), the LDH leakages of cells treated with Au NPs, Au@HSA NPs, Au@HGG NPs, and Au@HSF NPs at 500 μM is nearly ignored (Figure S3), suggesting that Au NPs and Au@Protein NPs cause no damage to the integrity of the plasma membrane.

To investigate the effect of the Au@protein complexes on ATP levels,we measured the ATP level as the cells were treated with Au NPs, Au@HSA NPs, Au@HGG NPs, and Au@HSF NPs at a concentration of 500 μM for 3 h. As shown in Figure 6B, the ATP levels are nearly unchanged for the cells treated with Au NPs, Au@HGG NPs, and Au@HSF NPs. However, what's interesting is that the cells treated with Au@HSA NPs have an even lower ATP level than the control. Thus, as can be seen, instead of mitigating cytotoxicity induced by Au NPs, coating of the Au NPs with HSA corona accelerates the depletion of intracellular ATP.

DOI: 10.1021/acsami.5b05744
ACS Appl. Mater. Interfaces 2015, 7, 17614−17622

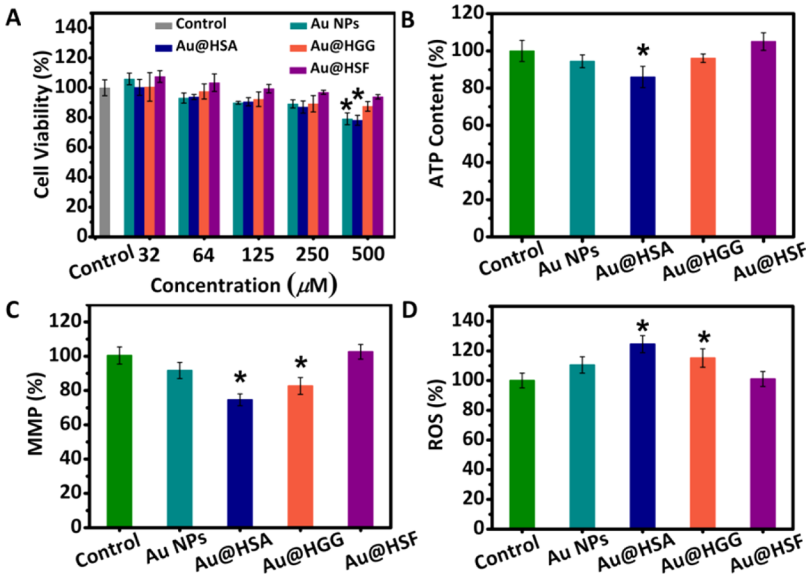

Figure 6. (A) The viability of HeLa cells after being treated with Au NPs, Au@HSA NPs, Au@HGG NPs, and Au@HSF NPs at different concentrations for 24 h. (B) Effect on cellular ATP content, (C) MMP, and (D) ROS amount in HeLa cells after 3 h exposure to Au NPs, Au@HSA NPs, Au@HGG NPs, and Au@HSF NPs at a concentration of 500 μM. Error bars indicate standard deviations from the mean from three independent experiments; statistically significant differences relative to control ($p < 0.05$) are indicated by asterisks.

It has been reported that the steep decline in cellular ATP levels may be the result of mitochondrial depolarization.[41] Therefore, the changes in MMP after the cells were exposed to Au NPs and Au NPs@protein coronas were also determined. The MMP was measured using lipophilic dye JC-1, which can enter the mitochondria, aggregate, and fluoresce red when MMP is high. When the MMP collapses, the dye can no longer accumulate within the mitochondria and will fluoresce green. By monitoring the transfer of the fluorescence color, changes in MMP can be detected. The relative proportion of red and green fluorescence is traditionally used to measure the degree of mitochondrial depolarization. Figure 6C shows the results from the assessment of the changes in the MMP level of HeLa cells treated with Au NPs, Au@HSA NPs, Au@HGG NPs, and Au@HSF NPs at a concentration of 500 μM for 3 h. The MMP of the cells treated with Au NPs slightly decreases. Surprisingly, coating of the Au NPs with HSA and HGG further decreases the MMP of the treated cells. Only the HSF corona suppresses the Au NP-induced change in the MMP. The MMP in the cells treated with Au@HSF NPs is comparable to that of untreated cells.

To deeply understand the cytotoxicity of the protein corona, we further determined the ROS because it is thought to push cellular physiology to the limits by inducing oxidative stress. Intracellular ROS can be tested with the cell-permeable probe molecule DCFH-DA, which becomes fluorescent upon oxidation by intracellular ROS. As shown in Figure 6D, the cells treated with Au NPs have a slight increase in the ROS level compared to that of the untreated cells. Whereas, after being exposed to Au@HSA NPs and Au@HGG NPs, the ROS production in the cells is further increased. Only the cells treated with Au@HSF NPs produce a similar ROS level as that of the untreated cells. The changes in cellular ROS upon exposure to the three types of Au@protein coronas are in good agreement with the observed MMP effects. As some reports say, reduced MMP will lead to the overproduction of ROS and then break oxidation-antioxidant balance of normal ROS metabolism.[41−43]

A decrease in MMP has been observed in response to many stimuli, such as depletion of intracellular glutathione and protein thiols, possibly due to direct binding of nanoparticles.[44,45] According to our discussion, the enzymatic degradation of protein corona is accompanied by the competitive adsorption of other biomolecules through two possible pathways. First, molecules with higher affinity could adsorb onto Au NPs by spontaneously displacing the protein corona. Second, when the corona is largely degraded by proteinase and detached from Au NPs, the surface of Au NPs will be exposed to other biomolecules, including the thiol-containing molecules, which results in their adsorption. This could probably reduce the intracellular concentration of free thiol-containing molecules, such as glutathione. Because glutathione is an endogenous inhibitor of permeability transition pore complex (PTPC) opening,[46] its depletion will lead to the loss of MMP due to the opening of PTPC and the release of pro-apoptotic proteins, such as cytochrome *c*. A decreased MMP might uncouple the cascade of reactions in the oxidative phosphorylation chain and thus not only inhibit ATP production but also increase intracellular ROS production. For instance, the release of cytochrome *c* will lead to a breakdown in the mitochondrial electron flow and result in an increase in the ROS level and inefficient ATP production.[46,47] It is thus reasonable to deduce that a faster degradation rate of protein corona may accelerate the depletion of intracellular glutathione and result in lower ATP production, lower MMP, and higher ROS levels.

4. CONCLUSIONS

In the present work, we investigated the proteolytic degradation of Au NPs@protein corona complexes and their subsequent effects on cytotoxicity. The results showed that the enzymatic degradation rate of the protein corona formed by different proteins varied. It was sequentially increased for the Au@HSF, Au@HGG, and Au@HSA coronas. Degradation of the protective corona resulted in aggregation of the Au NPs. The intracellular study also suggested a much faster degradation of

DOI: 10.1021/acsami.5b05744
ACS Appl. Mater. Interfaces 2015, 7, 17614−17622

the Au@HSA corona than those of Au@HSF and Au@HGG coronas in living HeLa cells. The cytotoxicity assessment determined that the cell viability, ROS production, and amount of ATP and MMP were significantly affected after the cells were treated with Au@HSA NPs, whereas the HSF corona obviously inhibited the effect of Au NPs on cell viability, ATP content, MMP, and ROS levels. The difference in the enzymatic degradation rate for the different coronas might result in a difference in the induction of cytotoxicity.

■ ASSOCIATED CONTENT

Supporting Information

The Supporting Information is available free of charge on the ACS Publications website at DOI: 10.1021/acsami.5b05744.

Competitive adsorption evaluation and enzymatic degradation of the protein corona in DMEM; zeta potentials and dynamic light scattering diameters of Au NPs, Au@HSA-FITC NPs, Au@HGG-FITC NPs, and Au@HSF-FITC NPsp, LDH leakage assay, and supporting discussions. (PDF)

■ AUTHOR INFORMATION

Corresponding Author

*Phone: +86 431 85262426; Fax: +86 431 85685653; E-mail: jiangxiue@ciac.ac.cn.

Notes

The authors declare no competing financial interest.

■ ACKNOWLEDGMENTS

This work was financially supported by the National Natural Science Foundation of China for Excellent Young Scholar of China (21322510), National Natural Science Foundation of China (91227114), and Science and Technology Innovation Foundation of Jilin Province for Talents Cultivation (Grants 20150519014JH).

■ REFERENCES

(1) Yao, J.; Yang, M.; Duan, Y. Chemistry, Biology, and Medicine of Fluorescent Nanomaterials and Related Systems: New Insights into Biosensing, Bioimaging, Genomics, Diagnostics, and Therapy. *Chem. Rev.* **2014**, *114*, 6130−6178.

(2) Park, M. V. D. Z.; Neigh, A. M.; Vermeulen, J. P.; de la Fonteyne, L. J. J.; Verharen, H. W.; Briedé, J. J.; van Loveren, H.; de Jong, W. H. The Effect of Particle Size on the Cytotoxicity, Inflammation, Developmental Toxicity and Genotoxicity of Silver Nanoparticles. *Biomaterials* **2011**, *32*, 9810−9817.

(3) Kim, S. T.; Saha, K.; Kim, C.; Rotello, V. M. The Role of Surface Functionality in Determining Nanoparticle Cytotoxicity. *Acc. Chem. Res.* **2013**, *46*, 681−691.

(4) Yu, T.; Greish, K.; McGill, L. D.; Ray, A.; Ghandehari, H. Influence of Geometry, Porosity, and Surface Characteristics of Silica Nanoparticles on Acute Toxicity: Their Vasculature Effect and Tolerance Threshold. *ACS Nano* **2012**, *6*, 2289−2301.

(5) Huang, X.; Li, L.; Liu, T.; Hao, N.; Liu, H.; Chen, D.; Tang, F. The Shape Effect of Mesoporous Silica Nanoparticles on Biodistribution, Clearance, and Biocompatibility in Vivo. *ACS Nano* **2011**, *5*, 5390−5399.

(6) Fleischer, C. C.; Payne, C. K. Nanoparticle−Cell Interactions: Molecular Structure of the Protein Corona and Cellular Outcomes. *Acc. Chem. Res.* **2014**, *47*, 2651−2659.

(7) Treuel, L.; Brandholt, S.; Maffre, P.; Wiegele, S.; Shang, L.; Nienhaus, G. U. Impact of Protein Modification on the Protein Corona on Nanoparticles and Nanoparticle−Cell Interactions. *ACS Nano* **2014**, *8*, 503−513.

(8) Yan, Y.; Gause, K. T.; Kamphuis, M. M. J.; Ang, C.-S.; O'Brien-Simpson, N. M.; Lenzo, J. C.; Reynolds, E. C.; Nice, E. C.; Caruso, F. Differential Roles of the Protein Corona in the Cellular Uptake of Nanoporous Polymer Particles by Monocyte and Macrophage Cell Lines. *ACS Nano* **2013**, *7*, 10960−10970.

(9) Tenzer, S.; Docter, D.; Kuharev, J.; Musyanovych, A.; Fetz, V.; Hecht, R.; Schlenk, F.; Fischer, D.; Kiouptsi, K.; Reinhardt, C.; Landfester, K.; Schild, H.; Maskos, M.; Knauer, S. K.; Stauber, R. H. Rapid Formation of Plasma Protein Corona Critically Affects Nanoparticle Pathophysiology. *Nat. Nanotechnol.* **2013**, *8*, 772−781.

(10) Salvati, A.; Pitek, A. S.; Monopoli, M. P.; Prapainop, K.; Bombelli, F. B.; Hristov, D. R.; Kelly, P. M.; Aberg, C.; Mahon, E.; Dawson, K. A. Transferrin-Functionalized Nanoparticles Lose Their Targeting Capabilities When a Biomolecule Corona Adsorbs on the Surface. *Nat. Nanotechnol.* **2013**, *8*, 137−143.

(11) Lynch, I.; Salvati, A.; Dawson, K. A. Protein-Nanoparticle Interactions: What Does the Cell See? *Nat. Nanotechnol.* **2009**, *4*, 546−547.

(12) Monopoli, M. P.; Aberg, C.; Salvati, A.; Dawson, K. A. Biomolecular Coronas Provide the Biological Identity of Nanosized Materials. *Nat. Nanotechnol.* **2012**, *7*, 779−786.

(13) Casals, E.; Pfaller, T.; Duschl, A.; Oostingh, G. J.; Puntes, V. F. Hardening of the Nanoparticle-Protein Corona in Metal (Au, Ag) and Oxide (Fe_3O_4, CoO, and CeO_2) Nanoparticles. *Small* **2011**, *7*, 3479−3486.

(14) Safi, M.; Courtois, J.; Seigneuret, M.; Conjeaud, H.; Berret, J. F. The Effects of Aggregation and Protein Corona on the Cellular Internalization of Iron Oxide Nanoparticles. *Biomaterials* **2011**, *32*, 9353−9363.

(15) Jiang, X.; Weise, S.; Hafner, M.; Röcker, C.; Zhang, F.; Parak, W. J.; Nienhaus, G. U. Quantitative Analysis of The Protein Corona on FePt Nanoparticles Formed by Transferrin Binding. *J. R. Soc., Interface* **2010**, *7*, S5−S13.

(16) Mortensen, N. P.; Hurst, G. B.; Wang, W.; Foster, C. M.; Nallathamby, P. D.; Retterer, S. T. Dynamic Development of the Protein Corona on Silica Nanoparticles: Composition and Role in Toxicity. *Nanoscale* **2013**, *5*, 6372−6380.

(17) Roach, P.; Farrar, D.; Perry, C. C. Surface Tailoring for Controlled Protein Adsorption: Effect of Topography at the Nanometer Scale and Chemistry. *J. Am. Chem. Soc.* **2006**, *128*, 3939−3945.

(18) Lundqvist, M.; Stigler, J.; Elia, G.; Lynch, I.; Cedervall, T.; Dawson, K. A. Nanoparticle Size and Surface Properties Determine the Protein Corona with Possible Implications for Biological Impacts. *Proc. Natl. Acad. Sci. U. S. A.* **2008**, *105*, 14265−14270.

(19) Bai, J.; Wang, T. T.; Wang, Y. C.; Jiang, X. E. Effects of Nanoparticle Surface Ligands on Protein Adsorption and Subsequent Cytotoxicity. *Biomater. Sci.* **2014**, *2*, 493−501.

(20) Rocker, C.; Potzl, M.; Zhang, F.; Parak, W. J.; Nienhaus, G. U. A Quantitative Fluorescence Study of Protein Monolayer Formation on Colloidal Nanoparticles. *Nat. Nanotechnol.* **2009**, *4*, 577−580.

(21) Sahoo, B.; Goswami, M.; Nag, S.; Maiti, S. Spontaneous Formation of a Protein Corona Prevents the Loss of Quantum Dot Fluorescence in Physiological Buffers. *Chem. Phys. Lett.* **2007**, *445*, 217−220.

(22) Jiang, X.; Zuber, A.; Heberle, J.; Ataka, K. In Situ Monitoring of the Orientated Assembly of Strep-Tagged Membrane Proteins on the Gold Surface by Surface Enhanced Infrared Absorption Spectroscopy. *Phys. Chem. Chem. Phys.* **2008**, *10*, 6381−6387.

(23) Ma, Z. F.; Bai, J.; Wang, Y. C.; Jiang, X. Impact of Shape and Pore Size of Mesoporous Silica Nanoparticles on Serum Protein Adsorption and RBCs Hemolysis. *ACS Appl. Mater. Interfaces* **2014**, *6*, 2431−2438.

(24) Liu, W.; Rose, J.; Plantevin, S.; Auffan, M.; Bottero, J.-Y.; Vidaud, C. Protein Corona Formation for Nanomaterials and Proteins of a Similar Size: Hard or Soft Corona? *Nanoscale* **2013**, *5*, 1658−1668.

(25) Walkey, C. D.; Olsen, J. B.; Guo, H. B.; Emili, A.; Chan, W. C. W. Nanoparticle Size and Surface Chemistry Determine Serum

DOI: 10.1021/acsami.5b05744
ACS Appl. Mater. Interfaces 2015, 7, 17614−17622

Protein Adsorption and Macrophage Uptake. *J. Am. Chem. Soc.* **2012**, *134*, 2139−2147.
(26) Lundqvist, M.; Stigler, J.; Cedervall, T.; Berggård, T.; Flanagan, M. B.; Lynch, I.; Elia, G.; Dawson, K. The Evolution of the Protein Corona around Nanoparticles: A Test Study. *ACS Nano* **2011**, *5*, 7503−7509.
(27) Wang, L.; Liu, Y.; Li, W.; Jiang, X.; Ji, Y.; Wu, X.; Xu, L.; Qiu, Y.; Zhao, K.; Wei, T.; Li, Y.; Zhao, Y.; Chen, C. Selective Targeting of Gold Nanorods at the Mitochondria of Cancer Cells: Implications for Cancer Therapy. *Nano Lett.* **2011**, *11*, 772−780.
(28) Lartigue, L.; Wilhelm, C.; Servais, J.; Factor, C.; Dencausse, A.; Bacri, J.-C.; Luciani, N.; Gazeau, F. Nanomagnetic Sensing of Blood Plasma Protein Interactions with Iron Oxide Nanoparticles: Impact on Macrophage Uptake. *ACS Nano* **2012**, *6*, 2665−2678.
(29) Lesniak, A.; Fenaroli, F.; Monopoli, M. P.; Åberg, C.; Dawson, K. A.; Salvati, A. Effects of the Presence or Absence of a Protein Corona on Silica Nanoparticle Uptake and Impact on Cells. *ACS Nano* **2012**, *6*, 5845−5857.
(30) Barrán-Berdón, A. L.; Pozzi, D.; Caracciolo, G.; Capriotti, A. L.; Caruso, G.; Cavaliere, C.; Riccioli, A.; Palchetti, S.; Laganà, A. Time Evolution of Nanoparticle−Protein Corona in Human Plasma: Relevance for Targeted Drug Delivery. *Langmuir* **2013**, *29*, 6485−6494.
(31) Lesniak, A.; Campbell, A.; Monopoli, M. P.; Lynch, I.; Salvati, A.; Dawson, K. A. Serum Heat Inactivation Affects Protein Corona Composition and Nanoparticle Uptake. *Biomaterials* **2010**, *31*, 9511−9518.
(32) Albanese, A.; Walkey, C. D.; Olsen, J. B.; Guo, H.; Emili, A.; Chan, W. C. W. Secreted Biomolecules Alter the Biological Identity and Cellular Interactions of Nanoparticles. *ACS Nano* **2014**, *8*, 5515−5526.
(33) Wang, F.; Yu, L.; Monopoli, M. P.; Sandin, P.; Mahon, E.; Salvati, A.; Dawson, K. A. The Biomolecular Corona is Retained During Nanoparticle Uptake and Protects the Cells from the Damage Induced by Cationic Nanoparticles until Degraded in the Lysosomes. *Nanomedicine* **2013**, *9*, 1159−1168.
(34) Frens, G. Controlled Nucleation for the Regulation of the Particle Size in Monodisperse Gold Suspensions. *Nature, Phys. Sci.* **1973**, *241*, 20−22.
(35) Jiang, D.; Zhao, H.; Zhang, S.; John, R. Kinetic Study of Photocatalytic Oxidation of Adsorbed Carboxylic Acids at TiO_2 Porous Films by Photoelectrolysis. *J. Catal.* **2004**, *223*, 212−220.
(36) Pihlasalo, S.; Kirjavainen, J.; Hanninen, P.; Harma, H. Ultrasensitive Protein Concentration Measurement Based on Particle Adsorption and Fluorescence Quenching. *Anal. Chem.* **2009**, *81*, 4995−5000.
(37) Chen, S.-J.; Chang, H.-T. Nile Red-Adsorbed Gold Nanoparticles for Selective Determination of Thiols Based on Energy Transfer and Aggregation. *Anal. Chem.* **2004**, *76*, 3727−3734.
(38) Belyanskaya, L.; Manser, P.; Spohn, P.; Bruinink, A.; Wick, P. The Reliability and Limits of the MTT Reduction Assay for Carbon Nanotubes−Cell Interaction. *Carbon* **2007**, *45*, 2643−2648.
(39) Holder, A. L.; Goth-Goldstein, R.; Lucas, D.; Koshland, C. P. Particle-Induced Artifacts in the MTT and LDH Viability Assays. *Chem. Res. Toxicol.* **2012**, *25*, 1885−1892.
(40) Fraga, S.; Faria, H.; Soares, M. E.; Duarte, J. A.; Soares, L.; Pereira, E.; Costa-Pereira, C.; Teixeira, J. P.; de Lourdes Bastos, M.; Carmo, H. Influence of the Surface Coating on the Cytotoxicity, Genotoxicity and Uptake of Gold Nanoparticles in Human HepG2 Cells. *J. Appl. Toxicol.* **2013**, *33*, 1111−1119.
(41) Khan, M. I.; Mohammad, A.; Patil, G.; Naqvi, S. A. H.; Chauhan, L. K. S.; Ahmad, I. Induction of ROS, Mitochondrial Damage and Autophagy in Lung Epithelial Cancer Cells by Iron Oxide Nanoparticles. *Biomaterials* **2012**, *33*, 1477−1488.
(42) Pan, Y.; Leifert, A.; Ruau, D.; Neuss, S.; Bornemann, J.; Schmid, G.; Brandau, W.; Simon, U.; Jahnen-Dechent, W. Gold Nanoparticles of Diameter 1.4 nm Trigger Necrosis by Oxidative Stress and Mitochondrial Damage. *Small* **2009**, *5*, 2067−2076.
(43) Li, N.; Sioutas, C.; Cho, A.; Schmitz, D.; Misra, C.; Sempf, J.; Wang, M.; Oberley, T.; Froines, J.; Nel, A. Ultrafine Particulate Pollutants Induce Oxidative Stress and Mitochondrial Damage. *Environ. Health Perspect.* **2003**, *111*, 455−460.
(44) Liu, J.; Shen, H. M.; Ong, C. N. Role of Intracellular Thiol Depletion, Mitochondrial Dysfunction and Reactive Oxygen Species in Salvia Miltiorrhiza-Induced Apoptosis in Human Hepatoma HepG2 Cells. *Life Sci.* **2001**, *69*, 1833−1850.
(45) Yang, C. F.; Shen, H. M.; Ong, C. N. Intracellular Thiol Depletion Causes Mitochondrial Permeability Transition in Ebselen-Induced Apoptosis. *Arch. Biochem. Biophys.* **2000**, *380*, 319−330.
(46) Fulda, S.; Galluzzi, L.; Kroemer, G. Targeting Mitochondria for Cancer Therapy. *Nat. Rev. Drug Discovery* **2010**, *9*, 447−464.
(47) Zamzami, N.; Marchetti, P.; Castedo, M.; Decaudin, D.; Macho, A.; Hirsch, T.; Susin, S. A.; Petit, P. X.; Mignotte, B.; Kroemer, G. Sequential Reduction of Mitochondrial Transmembrane Potential and Generation of Reactive Oxygen Species in Early Programmed Cell Death. *J. Exp. Med.* **1995**, *182*, 367−377.

DOI: 10.1021/acsami.5b05744
ACS Appl. Mater. Interfaces 2015, 7, 17614−17622